Hydrogen generation from MgNdNiMg15 composites by hydrolysis reaction

Eliane Alasmar, Isabelle Aubert, A. Durand, Michel Nakhl, Mirvat Zakhour, Etienne Gaudin, Jean-Louis Bobet

Hydrogen generation from Mg–$NdNiMg_{15}$ composites by hydrolysis reaction

E. Alasmar [a,b,c], *I. Aubert* [d], *A. Durand* [b,c], *M. Nakhl* [a], *M. Zakhour* [a], *E. Gaudin* [b,c], *J.-L. Bobet* [b,c,*]

[a] *LCPM/PR2N (EDST), Université Libanaise, Faculté des Sciences II, 90656 Jdeidet El Metn, Lebanon*
[b] *CNRS, ICMCB, UPR 9048, F-33600 Pessac, France*
[c] *Univ. Bordeaux, ICMCB, UPR 9048, F-33600 Pessac, France*
[d] *Univ. Bordeaux, CNRS, I2M, UMR 5295, F-33400 Talence, France*

ABSTRACT

The effects of the Mg content on the microstructure and hydrogen generation kinetics of Mg–$NdNiMg_{15}$ composites by hydrolysis reaction in seawater (3.5 wt% NaCl) was investigated. The presence of $NdNiMg_{15}$ in Mg matrix promotes galvanic corrosion. Thus, a galvanic coupling was observed between the $NdNiMg_{15}$ phase (cathode) and the Mg phase (anode). An acceleration of the corrosion rate of Mg phase was observed due to this galvanic coupling. Electrochemical tests confirm that pure Mg has a corrosion rate in salt water up to 750 times lower than that of the Mg phase in the Mg–$NdNiMg_{15}$ 90% composite. The best hydrolysis performance (100% of the theoretical hydrogen generation yield in slightly more than 15 min) observed for Mg–$NdNiMg_{15}$ 90% composite, was explained by a combined effect of galvanic corrosion, intergranular corrosion and pitting corrosion.

Introduction

Hydrogen is considered as a promising energy carrier because of its high energy density (142 MJ kg^{-1}), light weight (2 g ml^{-1}) and environmentally benign product of oxidation (water) [1,2]. Traditional methods which produce hydrogen from fossil fuel, or methanol are not suitable because of their CO_2 emissions [3]. Thus, many new hydrogen generation methods are proposed by researchers. Among these methods, hydrogen generation by the reaction of metal, metal alloy or metal compounds with water is becoming an important research area [4–6]. In particular, hydrolysis of Mg-based materials has attracted many researcher's attention [7–9]. Magnesium is a very promising hydrolyzing material due to its low density, high capacity, good activity and abundance in the earth. These materials generate hydrogen according to the following well known reaction (Eq. (1)):

$$Mg + 2H_2O \rightarrow Mg(OH)_2 + H_2 \quad (1)$$

Which can be split in an anodic reaction (2) and a cathodic one (3)

$$Mg \rightarrow Mg^{2+} + 2e^- \quad (2)$$

$$2H_2O + 2e^- \rightarrow H_2 + 2OH^- \quad (3)$$

* *Corresponding author*. CNRS, ICMCB, UPR 9048, F-33600 Pessac, France.
E-mail address: jean-louis.bobet@u-bordeaux.fr (J.-L. Bobet).

Thus, the hydrogen generation rate of Mg is proportional to its corrosion rate in water. However, the formation of a passive magnesium hydroxide layer on the unreacted Mg surface rapidly stops the reaction. In the presence of Cl^- ions, $MgCl_2$ is formed locally on the surface of Mg by replacement of OH^- ions of $Mg(OH)_2$ by Cl^- ions, which leads to pitting corrosion [8,10]. Thus, hydrogen generation from the hydrolysis reaction of Mg easily and conveniently occurs in seawater. In addition, several authors have demonstrated that ball milling improves the hydrolysis performances of Mg composites [11–13]. Because Mg powder is dangerous when in contact with moisture and heat, bulk Mg has also been investigated [5,14–16].

Accordingly, development of safe Mg based materials with improved hydrogen generation rate compared to pure magnesium need to be developed. According to Eqs. (2) and (3), one strategy to increase the corrosion rate, and thus the hydrogen production rate, is to precipitate an electrochemical cathodic phase which will cause a galvanic corrosion with the anodic Mg matrix [16]. The notion of micro-galvanic corrosion between the matrix and reinforcement has been documented in some of the earliest classical works on the corrosion of Mg based materials [17]. Recently SeKwon Oh *et al.* [15,16] showed that Mg-2.7Ni and Mg–Ni–Sn alloys exhibited faster hydrogen generation kinetics than pure Mg in seawater. For Mg-2.7Ni alloy, an electrochemically noble phase (Mg_2Ni) is formed at the grain boundaries and induced both galvanic and intergranular corrosions, which contributed to the acceleration of the hydrolysis rate. For Mg–Ni–Sn alloy, the Mg_2Sn and Mg_2Ni are formed along the grain boundaries and acted as an initiation site for pitting corrosion and as a cathode for both corrosion and intergranular corrosions.

Recently, $NdNiMg_{15}$ a very rich Mg compound, has been discovered by our group. Up to now, it is the richest Mg ordered ternary crystalline phase ever discovered. It crystallizes in the tetragonal system, *P4/nmm* (Z = 2) with the following set of parameters: $a = 10.0602(1)$ Å, $c = 7.7612(2)$ Å leading to a density of $d_{calc} = 2.40\ g\ cm^{-3}$. In our previous work [13,18], we studied the hydrolysis reaction of $NdNiMg_{15}$ ternary compound. Nevertheless, the maximum yield of this compound does not exceed 60%.

In this work, the effects of the Mg content on the microstructure and hydrogen production kinetics by hydrolysis in seawater (3.5 wt% NaCl) was investigated. Thus Mg–$NdNiMg_{15}$ composites have been synthesized. The compound $NdNiMg_{15}$ corresponds to 64 wt% of Mg, therefore by increasing the weight percentage in Mg to 70 wt% (molar composition: (1Nd + 1 Ni + 15Mg) + 4.6Mg), 80 wt% ((1Nd + 1 Ni + 15Mg) + 18.4Mg) and 90 wt% ((1Nd + 1 Ni + 15Mg) + 60Mg), we obtained Mg–$NdNiMg_{15}$ composites. These composites are named according to the total weight percentage of Mg (*i.e.* Mg–$NdNiMg_{15}$ x%, x is the total weight percentage of Mg).

Experiments

The Mg–$NdNiMg_{15}$ composites were prepared using neodymium pieces, nickel rods, and magnesium rods (all purities higher than 99.8%) as starting materials. The details of the synthesis were reported in previous paper for the $NdNiMg_5$ phase [19]. The hydrolysis reaction was carried out in a salted water solution (3.5 wt % NaCl) and more details can be found in reference [9]. The samples were characterized by X-ray diffraction (XRD) using a Philips PANalyticalX'Pert (PW1820) diffractometer with Cu $K_{\alpha 1}$ radiation ($\lambda = 1.5405$ Å). Scanning Electron Microscopy (SEM) observations were made using a TESCAN VEGA3 SB and SERON TECHNOLOGY microscopes.

Before corrosion tests, the compacted samples were mechanically polished up to 4000 grit SiC paper with ethanol as lubricant. A delay of 5 min was observed between the polishing and the electrochemical measurements in 3.5 wt% NaCl solution. The exposed surface sample of about 1 cm^2 was accurately measured before each test. A three-electrode cell was used including the magnesium alloy specimen as the working electrode, a titanium grid as the counter electrode and a saturated calomel electrode (SCE) as the reference electrode, all of them being connected to a potentiostat Ametek VersaSTAT 3F. All of the potentials quoted in this work are related to the SCE reference. Open circuit potential (OCP) measurements were performed for 30 min, corresponding to the time required for potential stabilization. The anodic and the cathodic portions of the polarization curves were plotted separately. For the anodic portion, the sample was maintained for 30 min at OCP, then, the potential was switched to (OCP − 20 mV) and scanned up to (OCP + 280 mV). After the anodic part measurements, the solution was changed, the sample was polished up to 4000 grit SiC paper and 5 min delay were observed before the following measurements. For the cathodic portion, the sample was maintained for 30 min at OCP, and then, the potential was switched to (OCP + 20 mV) and scanned up to (OCP − 280 mV). The scan rate was 0.5 mV/s for both parts of the polarization curve. All electrochemical tests (OCP and polarization curves) were repeated at least three times to ensure the reproducibility of the measurements.

Results

Microstructures of the Mg–$NdNiMg_{15}$ composites

Fig. 1 shows the results of the Electron Probe Micro-Analysis (EPMA) of Mg–$NdNiMg_{15}$ composites.

The chemical composition deduced from the EPMA (WDS detector) shows that the dark contrast corresponds to the Mg phase, while the $NdNiMg_{15}$ phase is the one that appears in brightest contrast. We can notice that, as the weight percentage of Mg increase, Mg dendrites become more numerous and larger (Fig. 1(b) and (c)), and the $NdNiMg_{15}$ phase surrounding them becomes thinner. Thus, for the Mg–$NdNiMg_{15}$ 90% composite, a five microns thick layer of $NdNiMg_{15}$ phase surrounds grain boundaries of Mg. From image analysis, we can accurately calculate the surface percentages of NdNiMg15 phase which are 78% for the Mg–$NdNiMg_{15}$ 70% composite, 48% for the Mg–$NdNiMg_{15}$ 80% composite and only 22% for the Mg–$NdNiMg_{15}$ 90% composite. The surface percentages are in very good agreement with the volume and molar percentages calculated from the phase diagram.

The atomic mapping (Fig. 2) of the elements (Nd, Ni and Mg) of the composites (*e.g.* Mg–$NdNiMg_{15}$ 80 and 90% in Fig. 2(a)

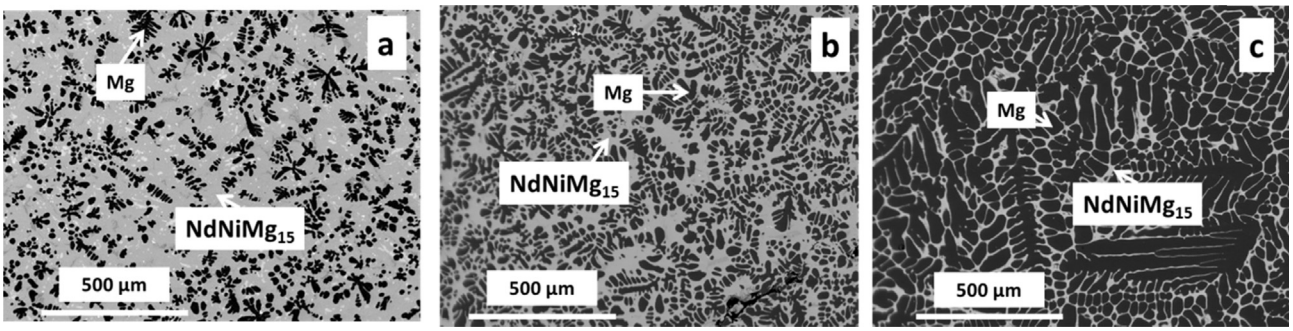

Fig. 1 – Electron Probe Micro-Analysis (BSE surface images) of Mg –$NdNiMg_{15}$ a) 70% and b) 80% c) 90% composites.

and (b) respectively) confirms the presence of the two phases ($NdNiMg_{15}$ and Mg).

The X-Ray diffraction patterns of Mg–$NdNiMg_{15}$ composites (Fig. 3) reveal peaks related to $NdNiMg_{15}$ and Mg phases. The characteristic peaks of Mg are mainly those observed at $2\theta = 32.2°$, 34.4° and 36.6°. As expected, the intensity of Mg peaks increases when the weight percentage of Mg increases, while thus related to $NdNiMg_{15}$ decrease. The lattice parameters of NdNiMg15 compounds are almost the same whatever the Mg content in the composites (*i.e.* for the composites with 70, 80 and 90 Mg%: $a = 10.060$ (1) Å, $c = 7.761(1)$; $a = 10.061$ (1) Å, $c = 7.760(1)$; $a = 10.060$ (1) Å, $c = 7.760(1)$). This results was also confirm by the EMPA analysis (not presented here). The only difference between the composites (except the variation of the $NdNiMg_{15}$/Mg ratio) is the presence and quantity (still very low) of the 2 impurities: $Mg_{12}Nd$ and $Nd_4Ni_8Mg_{80}$.

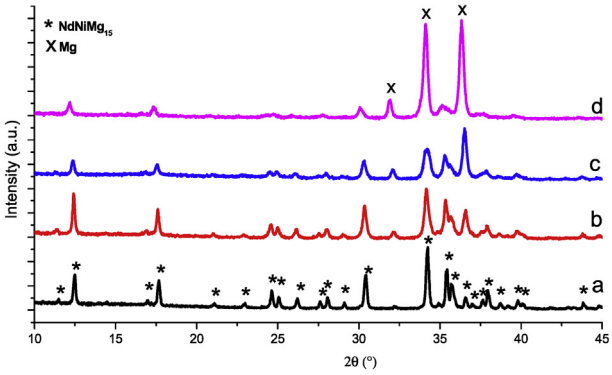

Fig. 3 – XRD patterns of the a) $NdNiMg_{15}$ compound compared to the Mg–$NdNiMg_{15}$ b) 70% c) 80% and d) 90% composites.

Hydrogen generation from Mg–$NdNiMg_{15}$ composites

Fig. 4 shows a comparison between $NdNiMg_{15}$, Mg and Mg–$NdNiMg_{15}$ composites in term of hydrogen generation yield. Before the hydrolysis reaction, all samples are hand milled for less than a minute in an agate mortar.

It can be seen that all samples have an improved yield and kinetics compared to pure magnesium whose reaction stops after 800 s and has a yield of only 12%. As the Mg content increases, the theoretical hydrogen production yield and hydrogen generation kinetics increase. Thus, Mg–$NdNiMg_{15}$ 90% composite has the best hydrolysis performance, despite

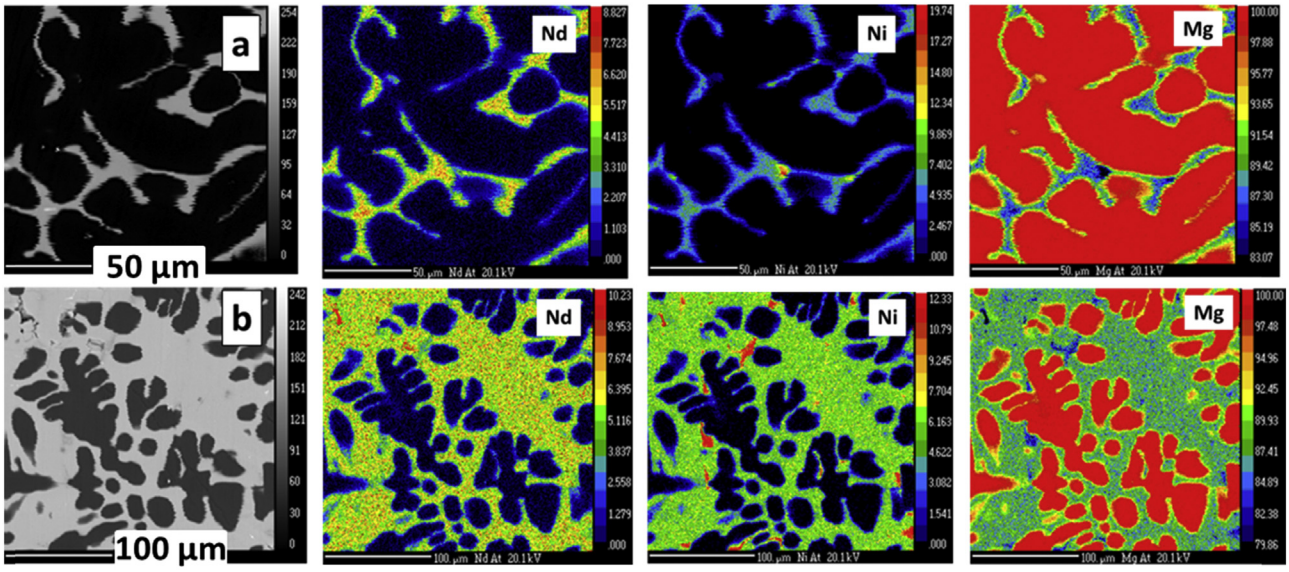

Fig. 2 – Atomic mapping of Mg–$NdNiMg_{15}$ a) 90% and b) 80% composites.

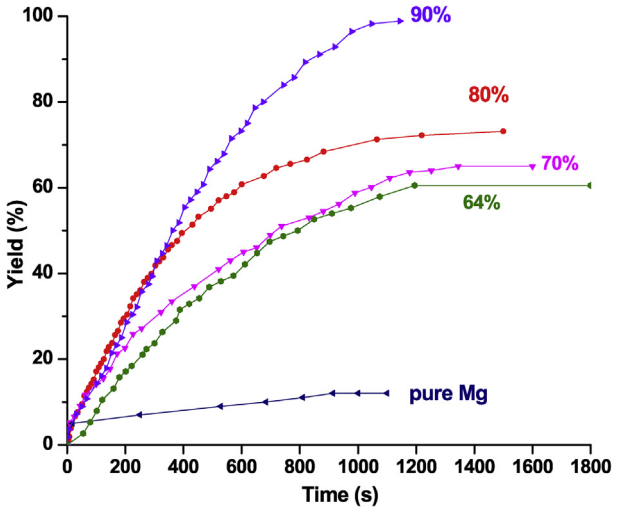

Fig. 4 – Hydrogen generation yield for Mg–$NdNiMg_{15}$ composites compared to $NdNiMg_{15}$ and pure Mg in salted water (NaCl 3.5 wt%).

the small amount of Ni and Nd. Referring to Fig. 4, Mg–$NdNiMg_{15}$ 90% composite release 100% of the theoretical hydrogen generation yield in slightly more than 15 min. The kinetics of hydrogen production is significantly higher for the composite Mg–$NdNiMg_{15}$ 90% (*i.e.* 60 ml g^{-} min^{-1}) compared to those for Mg-2.7Ni (23.8 ml g^{-1} min^{-1}) and Mg - 2.7Ni - 1Sn (28.7 ml g^{-1} min^{-1}) as well as for pure Mg (0.017 ml g^{-1} min^{-1}) reported by Sekwon *et al.* [15,16]. This should be attributed to the presence of the $NdNiMg_{15}$ phase (in our case) at the Mg grain boundaries.

The solid products remaining after hydrolysis of $NdNiMg_{15}$ compound and Mg–$NdNiMg_{15}$ composites were characterized by XRD (Fig. 5). After hydrolysis, the peaks related to magnesium hydroxide appear as well as thus related to NaCl. For $NdNiMg_{15}$ compound and Mg–$NdNiMg_{15}$ 70 and 80% composites, peaks related to $NdNiMg_{15}$ are still present which confirms the non-complete reaction. For the composite Mg–$NdNiMg_{15}$ 90%, no peak related to $NdNiMg_{15}$ is observed confirming the complete reaction (and so the 100% yield reported in Fig. 4).

Electrochemical tests

A) Open Circuit Potential (OCP).

The effect of the presence of $NdNiMg_{15}$ in Mg matrix was studied by electrochemical means. The Open Circuit Potential variations as a function of time (OCP, Fig. 6) were recorded for Mg–$NdNiMg_{15}$ composites and compared to those of Mg and $NdNiMg_{15}$ (*i.e.* 64 wt% Mg) compounds. The corrosion potentials were calculated from OCP measurements by averaging OCP values from 1500 s to 1800 s of immersion. Corrosion potentials of the different alloys are summarized in Table 1.

The OCP value increases during the first 100 s and then stabilizes around 500 s, that corresponds to the initiation time of dark pits. After 500 s, the surface turns to black without OCP modification up to 30 min of immersion for samples containing the $NdNiMg_{15}$ phase, while it takes about 6 h to pure magnesium to present a similar appearance (Fig. 7). Curioni *et al.* [20] showed that the dark zones correspond to layers of chloride-rich hydroxides. Indeed, at the beginning of the test, the sample surface was shiny and protected by the air-formed $Mg(OH)_2$ hydroxide. But during immersion in salt water, $Mg(OH)_2$ was replaced by $MgCl_2$ which was formed locally on the surface of Mg by substitution of OH^- ions of $Mg(OH)_2$ by Cl^- ions. The dark $MgCl_2$ layer formed locally on the Mg surface

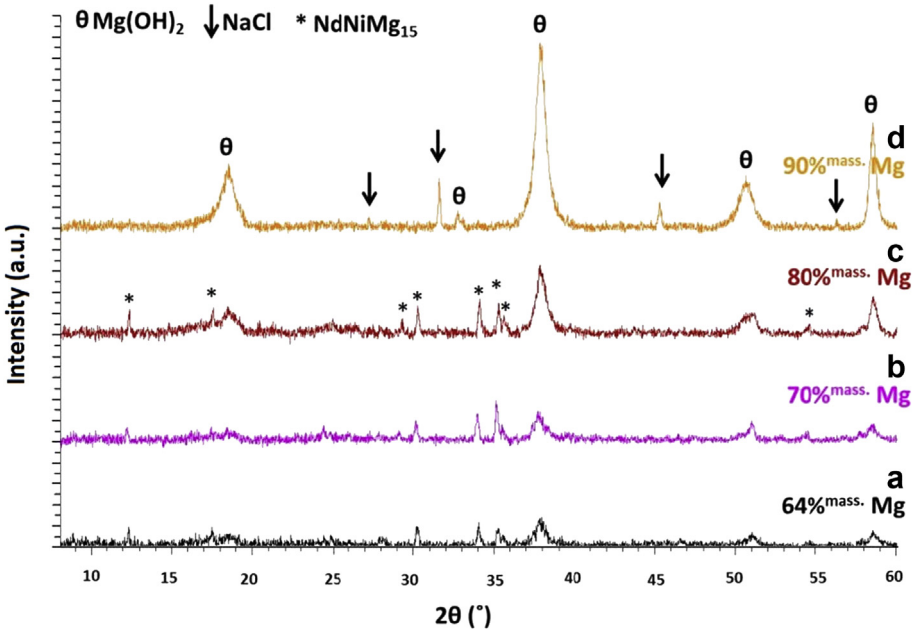

Fig. 5 – X-ray diffraction patterns for the hydrolysis product of the a) compound $NdNiMg_{15}$ compared to the composites Mg–$NdNiMg_{15}$ b) 70% c) 80% and d) 90%.

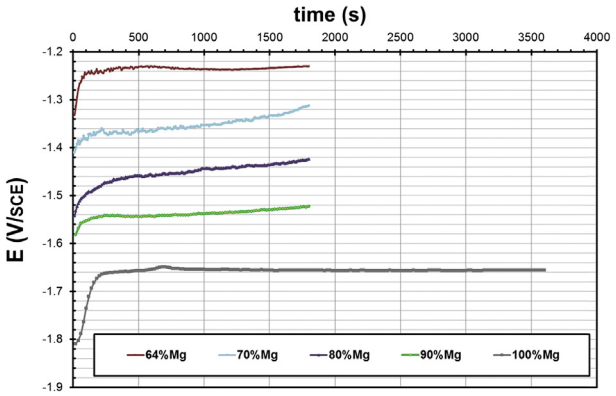

Fig. 6 – OCP measurement with time for Mg–NdNiMg$_{15}$ 70, 80 and 90% composites compared to NdNiMg$_{15}$ compound (64%) and pure Mg.

Table 1 – OCP values for Mg–NdNiMg$_{15}$ 70, 80 and 90% composites compared to NdNiMg$_{15}$ compound (64%) and pure Mg.

Samples (wt.% of Mg)	64	70	80	90	100
Corrosion potential Ecorr (V/ECS)	−1.23	−1.26	−1.44	−1.53	−1.65

could thus be easily dissolved because of the greater solubility of $MgCl_2$ in water compared to that of $Mg(OH)_2$ (*e.g.* $MgCl_2$: 542 g/L, $Mg(OH)_2$: 0.009 g/L at 20 °C). Anodic (2) and cathodic reactions (3) could occur on these dark areas resulting in pitting corrosion which progressively extended the entire surface.

The corrosion potential of Mg (Table 1) is in agreement with the values available in literature for Mg corrosion potential in salted water (*i.e.* −1.65) available in galvanic series in seawater [21–23]. The less cathodic corrosion potentials of the composites are due to the presence of the NdNiMg$_{15}$ phase which increases the corrosion potential to more anodic values. This has also been observed for AZ31 and AZ91 alloys [21], where the presence of beta phases increases the free potential.

It is possible to predict the galvanic couplings between both NdNiMg$_{15}$ and Mg from corrosion potential values. Indeed, the compound NdNiMg$_{15}$ (*i.e.* 64 wt% Mg) appears more cathodic than magnesium. The difference of corrosion potential is 0.42 V, which exceeds the 0.25 V required for galvanic coupling [24]. Such significant potential difference will therefore lead to a significant galvanic coupling at the microstructure scale between both phases leading to an accelerated corrosion. Furthermore, it is shown that intermetallic particles in Mg-alloys act generally as local cathodes [25]. Thus, in our composite, the NdNiMg$_{15}$ phase will constitute the cathode and Mg phase the anode.

B) Tafel plots.

In order to quantify the corrosion rate of each composite, polarization curves were plotted (Fig. 8).

For each sample, J_{corr} was determined from the polarization curves and the line plot of Tafel [17]. The different values of J_{corr} obtained are summarized in Table 2. The values of J_{corr} increase as the percentage of Mg increases, except for the pure Mg which presents lowest value. This suggests a lower corrosion resistance (or a higher corrosion rate) as the mass percentage of Mg increases from 64 wt% up to 90 wt%.

Thus, the corrosion rate (CR, in weight loss per day) can be deduced from Faraday law (I_{corr} = n.F.CR) according to Eq. (4):

$$CR\left(\frac{g}{day}\right) = \frac{I_{corr}}{nF} = \frac{J_{corr} * S * M * 3600 * 24}{2 * 96500} \quad (4)$$

With I_{corr} the corrosion current (A), J_{corr} the corrosion current density (A/m^2), S the analyzed surface (m^2), n the valence change, M the molar mass of the sample, F the Faraday constant (96485 C/mol). The obtained values are summarized in Table 2.

It is found that the pure Mg has a corrosion rate in salted water up to 750 times lower compared to the Mg phase in the Mg–NdNiMg$_{15}$ 90% composite. This demonstrates the importance of galvanic corrosion, caused by the potential difference of 0.42 V between the Mg and NdNiMg$_{15}$ phases. For other Mg alloys as AZ91, in which the beta phase accelerates the corrosion of the alpha Mg phase, the corrosion rate increases only by a factor of 10–20 [26,27].

However, all composites do not have the same corrosion rate despite the presence of the same two phases. The difference can be due to the morphology and then from the other corrosion mechanism occurring. Then, an analysis of the surface morphology after hydrolysis was undertaken.

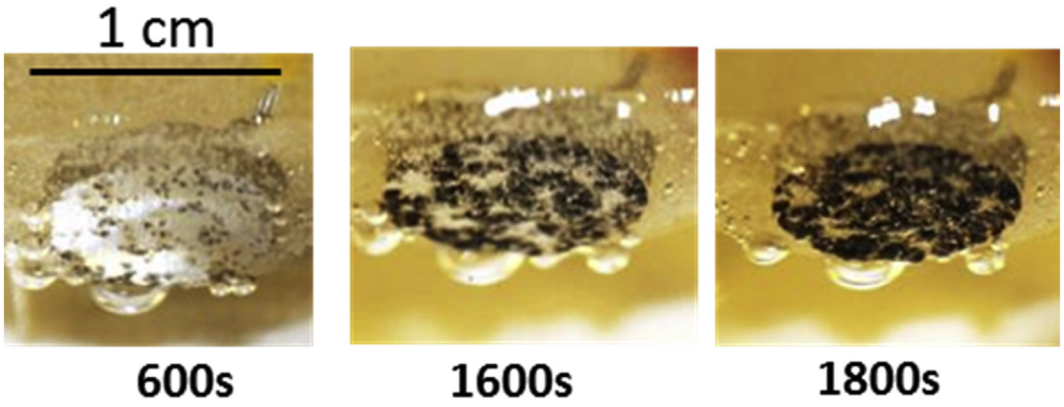

Fig. 7 – Surface modification during OCP measurement for Mg–NdNiMg$_{15}$ 80%.

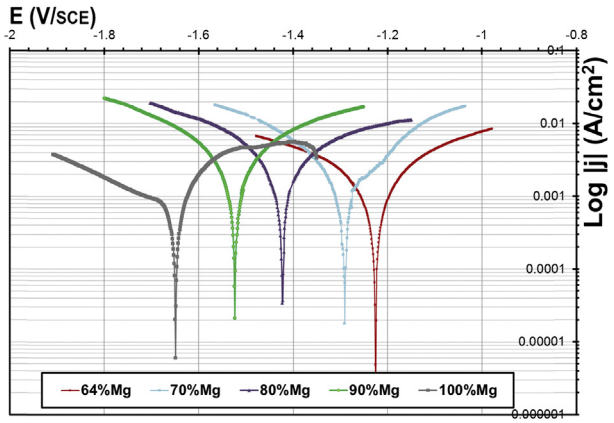

Fig. 8 – Polarization curves (Log $|j| = f(E)$) for Mg–$NdNiMg_{15}$ 70, 80 and 90% composites compared to $NdNiMg_{15}$ compound (64%) and pure Mg.

Table 2 – Corrosion current density (J_{corr}) and the corrosion rates of Mg–$NdNiMg_{15}$ 70, 80 and 90% composites compared to $NdNiMg_{15}$ compound (64%) and pure Mg.

Samples (wt.% of Mg)	64	70	80	90	100
J_{corr} (mA/cm^2)	1.76	3.71	4.66	4.96	0.558
CR (mg/day)	452	1180	2183	4503	6

Surface morphology after hydrolysis

Fig. 9 shows the surface morphology of Mg–$NdNiMg_{15}$ 90% composite before (Fig. 9(a)) and after 1 and 5 min of hydrolysis reaction (Fig. 9(b) and (c) respectively).

The SEM images (BSE) show the presence of cracks and products of corrosion at the Mg/$NdNiMg_{15}$ interfaces (Fig. 9 (b)). Indeed, at the microstructure scale, the contact between the anodic Mg phase and the cathodic $NdNiMg_{15}$ phase induced galvanic corrosion of Mg because of the significant difference in corrosion potential. As seen in Fig. 1, in the case of the Mg– $NdNiMg_{15}$ 90% composite, thin layers of cathodic $NdNiMg_{15}$ phase surrounded the Mg grains. The contact between the anodic and cathodic phases was then maximized and the galvanic corrosion of the Mg phase was enhanced at grain boundaries. That induced intergranular galvanic corrosion due to the segregation of $NdNiMg_{15}$ phase at the Mg grain boundaries. During the intergranular corrosion, the mass loss went in depth along the interface of the two phases which might lead to an increase in the effective area of the cathodic phase, and thus increase the galvanic corrosion [17]. In addition, after some time of immersion, the large production of hydrogen bubbles could extract some thin pieces of $NdNiMg_{15}$ phase around which galvanic corrosion had occurred (Fig. 9 (b)). Out of the alloy, the $NdNiMg_{15}$ phase could dissolve and result in the quasi-complete reaction.

After 5 min of immersion, a thick layer of corrosion products covered the surface (Fig. 9 (c)). But we can see that this layer contains a lot of cracks which allowed the continuation of the electrochemical activity.

According to the previous observations, we can assume that the significant increase in the hydrogen production of the Mg–$NdNiMg_{15}$ 90% composite is due to the combined effects of galvanic and intergranular corrosion. This hypothesis can be confirmed by the observation of surface without corrosion products.

Fig. 10 shows the SEM images (BSE) of the surface after 1 min of hydrolysis and etched in nital solution for 1 min (24 % volume distilled water, 75 %Volume ethylene glycol, 1 %

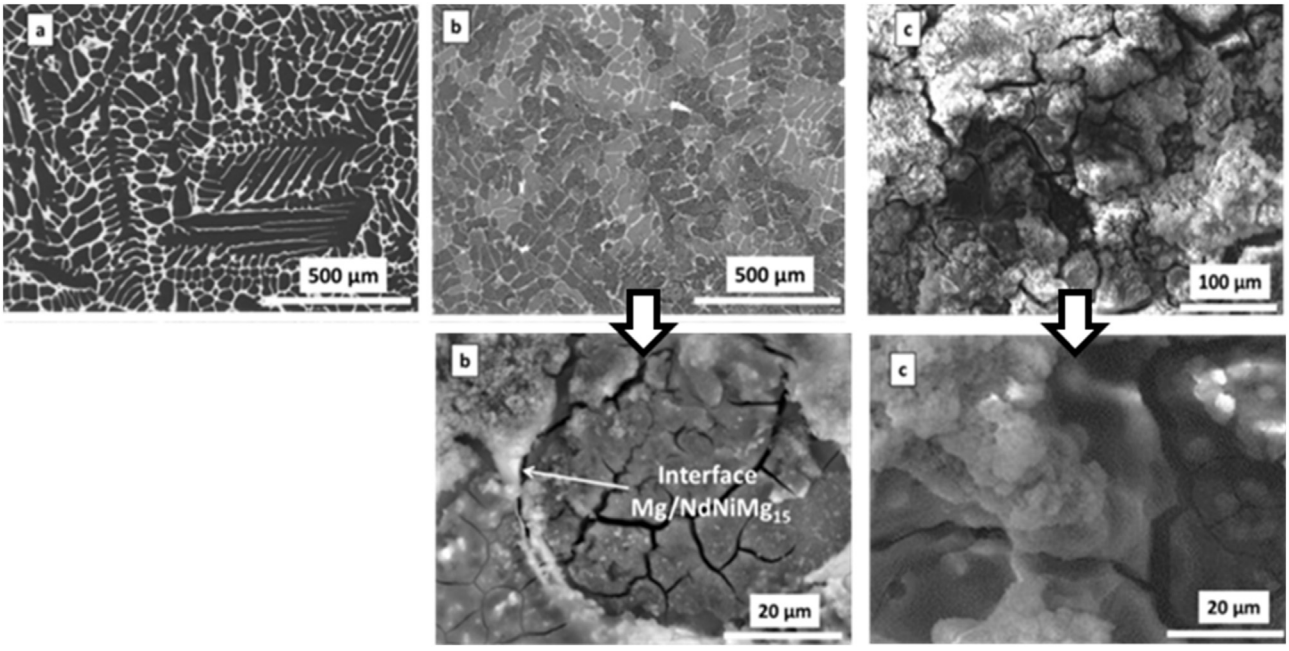

Fig. 9 – BSE Surface images of Mg–$NdNiMg_{15}$ 90% composite a) before and after b) 1 and c) 5 min of hydrolysis reaction.

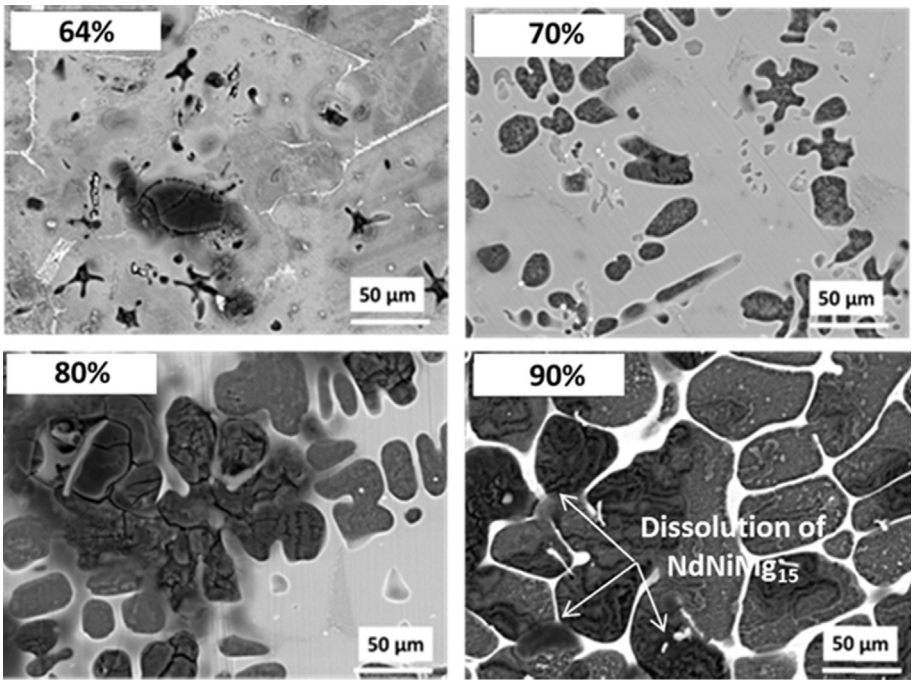

Fig. 10 – BSE surface images of Mg–$NdNiMg_{15}$ 70, 80 and 90% composites compared to $NdNiMg_{15}$ compound (64%) after 1 min of hydrolysis and etched in nital solution for 1 min.

Volume nitric acid; which allows the removal of the corrosion products formed on the surface).

Fig. 10 clearly demonstrates that $Mg(OH)_2$ layers are formed on the surface of Mg phase and are locally destroyed by pitting corrosion in the form of cracks or holes. We can also notice the preferential dissolution of Mg phase near the $NdNiMg_{15}$ phase, due to galvanic corrosion. The galvanic corrosion is more important in the case of Mg–$NdNiMg_{15}$ 90% composite in which the $NdNiMg_{15}$ phase finely surrounds the grain boundaries.

In addition, we can see that some pieces of $NdNiMg_{15}$ phase around which galvanic corrosion has occurred are missing, probably removed by the large production of hydrogen bubbles (some areas of the SEM micrographs marked by arrows, Fig. 9). This phenomenon is especially observed in the thinnest zones of this phase for Mg–$NdNiMg_{15}$ 90% composite. For composites Mg–$NdNiMg_{15}$ 80 and 70%, the cathodic phase is too thick for this to happen.

Thus, we can conclude that the pitting corrosion at the initiation stage and then galvanic and intergranular corrosion result in the best hydrolysis performance for the composite Mg–$NdNiMg_{15}$ 90%.

Moreover, the small amount of cathodic phase (22%) in this alloy can explain the complete hydrolysis reaction for the Mg–$NdNiMg_{15}$ 90% composite. Indeed, thin pieces of cathodic phase were removed from the alloy by the strong cathodic activity, and could corrode like the $NdNiMg_{15}$ compound. Although the maximum yield of this compound does not exceed 60%, the remaining small amount of cathodic phase did not affect the hydrogen generation yield. This phenomenon can explain the complete hydrolysis reaction for the Mg–$NdNiMg_{15}$ 90% composite.

Conclusion

Mg–$NdNiMg_{15}$ composites have been synthesized and it has been shown that it consists of both Mg and $NdNiMg_{15}$ phases. The effects of the Mg content on the microstructure and hydrogen production kinetics by hydrolysis in seawater (3.5 wt% NaCl) was investigated.

A galvanic coupling was observed between the $NdNiMg_{15}$ phase (cathode) and the Mg phase (anode) due to the difference in corrosion potential (−1.23 and −1.65 V respectively). For all composites, the corrosion rate of the Mg phase is increased and can be 750 times higher compared to the corrosion rate of pure Mg.

For the Mg–$NdNiMg_{15}$ 90% composite, the microstructure which is composed of a thin layer of $NdNiMg_{15}$ phase surrounding the grain boundaries of Mg results in the best hydrolysis performance, because of galvanic and intergranular corrosion; and this, despite the small amount of Ni and Nd. For Mg–$NdNiMg_{15}$ 80 and 70% composites, the hydrogen production yield is less important because of the weaker intervention of intergranular corrosion.

These results highlight that, to improve the hydrogen generation rate of Mg–$NdNiMg_{15}$ composites, it is important to promote the galvanic and intergranular corrosion with the formation of the $NdNiMg_{15}$ cathodic phase around the grain boundaries of the Mg anodic phase.

Acknowledgement

The authors would like to thank the Lebanese University and the Lebanese CNRS for funding this project through a grant for Eliane ALASMAR.

REFERENCES

[1] Sharma S, Ghoshal SK. Hydrogen the future transportation fuel: from production to applications. Renew Sustain Energy Rev 2015;43:1151e8.
[2] Veziroglu TN, S ,ahi_n S. 21st Century's energy: hydrogen energy system. Energy Convers Manag 2008;49(7):1820e31.
[3] Bertine KK, Goldberg ED. Fossil fuel combustion and the major sedimentary cycle. Science 1971;173(3993):233e5.
[4] Yang Y, Gai W-Z, Deng Z-Y. Hydrogen generation by the reaction of Al with water promoted by an ultrasonically prepared Al(OH) suspension. Int J Hydrogen Energy 2014;39(33):18734e42.
[5] Uan J-Y, Cho C-Y, Liu K-T. Generation of hydrogen from magnesium alloy scraps catalyzed by platinum-coated titanium net in NaCl aqueous solution. Int J Hydrogen Energy 2007;32(13):2337e43.
[6] Wang H, Leung D, Leung M. A review on hydrogen production using aluminum and aluminum alloys. Renew Sustain Energy Rev 2009;13(4):845e53.
[7] Grosjean MH, Zidoune M, Roue L. Hydrogen production from highly corroding Mg-based materials elaborated by ball milling. J Alloy Comp 2005;404-406:712e5.
[8] Awad AS, El-Asmar E, Tayeh T. Effect of carbons (G and CFs), TM (Ni, Fe and Al) and oxides (Nb 2 O 5 and V 2 O 5) on hydrogen generation from ball milled Mg-based hydrolysis reaction for fuel cell. Energy 2016;95:175e86.
[9] Tayeh T, Awad AS, Nakhl M. Production of hydrogen from magnesium hydrides hydrolysis. Int J Hydrogen Energy 2014;39(7):3109e17.
[10] Tunold R, Holtan H, Berge M-BH. The corrosion of magnesium in aqueous solution containing chloride ions. Corrosion Sci 1977;17(4):353e65.
[11] Zou M-S, Yang R-J, Guo X-Y. The preparation of Mg-based hydro-reactive materials and their reactive properties in seawater. Int J Hydrogen Energy 2011;36(11):6478e83.
[12] Grosjean M-H, Zidoune M, Roue L. Effect of ball milling on the corrosion resistance of magnesium in aqueous media. Electrochim Acta 2004;49(15):2461e70.
[13] Alasmar E, Awad AS, Hachem D. Hydrogen generation from Nd-Ni-Mg system by hydrolysis reaction. J Alloy Comp 2018;740:52e60.
[14] Cho C-Y, Wang K-H, Uan J-Y. Evaluation of a new hydrogen generating system: Ni-rich magnesium alloy catalyzed by platinum wire in sodium chloride solution. Mater Trans 2005;46(12):2704e8.
[15] Oh S, Cho T, Kim M. Fabrication of Mg —Ni—Sn alloys for fast hydrogen generation in seawater. Int J Hydrogen Energy 2017;42(12):7761e9.
[16] Oh S, Kim M, Eom K. Design of Mg —Ni alloys for fast hydrogen generation from seawater and their application in polymer electrolyte membrane fuel cells. Int J Hydrogen Energy 2016;41(10):5296e303.
[17] Esmaily M, Svensson JE, Fajardo S. Fundamentals and advances in magnesium alloy corrosion. Prog Mater Sci 2017;89:92e193.
[18] Al Asmar Eliane, Tence Sophie, Bobet Jean-Louis, Ourane Bassem, Nakhl Michel, Zakhour Mirvat, Gaudin Etienne. The Mg-rich phase NdNiMg15: structural and magnetic properties. Inorg Chem 2018;57:14152e8.
[19] Ourane B, Gaudin E, Lu YF. The new ternary intermetallic NdNiMg 5: hydrogen sorption properties and more. Mater Res Bull 2015;61:275e9.
[20] Curioni M. The behaviour of magnesium during free corrosion and potentiodynamic polarization investigated by real-time hydrogen measurement and optical imaging. Electrochim Acta 2014;120:284e92.
[21] Singh IB, Singh M, Das S. A comparative corrosion behavior of Mg, AZ31 and AZ91 alloys in 3.5% NaCl solution. J Magnes Alloy 2015;3(2):142e8.
[22] Creus J., technique de l'ingénieur: corrosion et protection des métaux en milieu marin, ed. C. 620.
[23] You J, Jingbi Y, Lei M. Improved air stability of perovskite solar cells via solution-processed metal oxide transport layers. Nat Nanotechnol 2016;11(1):75.
[24] Groysman A, editor. Corrosion in systems for storage and transportation of petroleum products. Springer; 2014.
[25] Su¨ dholz AD, Kirkland NT, Buchheit RG. Electrochemical properties of intermetallic phases and common impurity elements in magnesium alloys. Electrochem Solid State 2011;14:5e7.
[26] Song G, Atrens A. Understanding magnesium corrosion - a framework for improved alloy performance. Adv Eng Mater 2003;5:837e58.
[27] Song G, Atrens A. Corrosion mechanisms of magnesium alloys. Adv Eng Mater 1999;1:11e33.